Pharm Res
DOI 10.1007/s11095-012-0806-5

RESEARCH PAPER

Computational Prediction of CNS Drug Exposure Based on a Novel *In Vivo* Dataset

Christel A. S. Bergström • Susan A. Charman • Joseph A. Nicolazzo

Received: 19 April 2012 / Accepted: 8 June 2012

ABSTRACT

Purpose To develop a computational model for predicting CNS drug exposure using a novel *in vivo* dataset.

Methods The brain-to-plasma (B:P) ratio of 43 diverse compounds was assessed following intravenous administration to Swiss Outbred mice. B:P ratios were subjected to PLS modeling using calculated molecular descriptors. The obtained results were transferred to a qualitative setting in which compounds predicted to have a B:P ratio > 0.3 were sorted as high CNS exposure compounds and those below this value were sorted as low CNS exposure compounds. The model was challenged with an external test set consisting of 251 compounds for which semi-quantitative values of CNS exposure were available in the literature.

Results The dataset ranged more than 1700-fold in B:P ratio, with 16 and 27 compounds being sorted as low and high CNS exposure drugs, respectively. The model was a one principal component model based on five descriptors reflecting molecular shape, electronegativity, polarisability and charge transfer, and allowed 74% of the compounds in the training set and 76% of the test set to be predicted correctly.

Conclusion A qualitative computational model has been developed which accurately classifies compounds as being high or low CNS exposure drugs based on rapidly calculated molecular descriptors.

KEY WORDS blood–brain barrier · CNS exposure · computational model · *in silico* prediction · physicochemical properties

INTRODUCTION

In order for a therapeutic agent to exert its pharmacological effect on molecular targets within the brain, it must permeate the blood–brain barrier (BBB) following systemic administration. The BBB, which is formed by the endothelial cells lining cerebral microvessels, limits the entry of blood-borne agents into the brain through the presence of tight intercellular junctions (1,2), efflux transporters (3), and drug-metabolizing enzymes (4). Due to this restrictive nature, the brain uptake of compounds intended to treat disorders of the central nervous system (CNS) is often hindered. Indeed, it has been estimated that more than 98% of compounds intended to treat diseases of the CNS do not gain access to their target due to their inherent inability to cross the BBB (5,6). While this is a limitation for compounds intended to reach the CNS, this may be considered beneficial for those compounds whose site of action is peripheral,

Electronic supplementary material The online version of this article (doi:10.1007/s11095-012-0806-5) contains supplementary material, which is available to authorized users.

C. A. S. Bergström
Department of Pharmacy
Drug Optimization and Pharmaceutical Profiling Platform
Uppsala University, Uppsala Biomedical Center
P.O. Box 580, SE-751 23 Uppsala, Sweden

S. A. Charman
Centre for Drug Candidate Optimisation
Monash Institute of Pharmaceutical Sciences
Monash University
381 Royal Parade, Parkville, Victoria 3052, Australia

C. A. S. Bergström • J. A. Nicolazzo (✉)
Drug Delivery, Disposition and Dynamics
Monash Institute of Pharmaceutical Sciences
Monash University
381 Royal Parade, Parkville, Victoria 3052, Australia
e-mail: joseph.nicolazzo@monash.edu

Published online: 29 June 2012

thus minimizing the potential for neurotoxicity. Therefore, the ability of a compound to access the CNS needs to be assessed early in drug discovery, so that structural properties can be optimized to reach the desired effect (i.e. to either promote or hinder CNS exposure).

In order to assess the ability of compounds to permeate the BBB, various *in vitro* and *in vivo* models have been developed (7–11). While each of these models provides information on compound permeation, not all models are conducive to the moderate to high throughput setting required when screening small drug-like compound series as potential candidates. As a result, focus has turned to understanding the physicochemical and molecular properties of small drugs in an attempt to predict BBB permeability using computational models (12,13). Physicochemical parameters which have been shown to be important in contributing to BBB permeability include lipophilicity (14–16), polar surface area (15,17–19), molecular weight (14,19), number of H-bond donors and acceptors (18,19), and the number of free rotating bonds (20,21). As a consequence of these studies, some general guidelines have been developed suggesting that for BBB penetration, (i) the sum of nitrogen and oxygen atoms should be 5 or less, (ii) ClogP minus the number of nitrogen and oxygen atoms should be greater than 0 (where ClogP is the calculated logarithm of the partition coefficient between octanol and water), (iii) polar surface area should be less than 60–90 $Å^2$, (iv) molecular weight should be <450 Da, and (v) $\log D_{pH\ 7.4}$ should be in the range of 1–3 (12). While some of the above classification systems were based on experimental data, many predictive models have been solely based on classifying drugs as either CNS active or inactive, with no quantification of CNS exposure (17,19,20). The usage of CNS activity as a source for classification may not be reflective of the concentrations reaching the brain, as e.g. many compounds may permeate the BBB and exhibit no CNS activity given their inability to interact with relevant target receptors. Furthermore, where some models have been developed on experimental observations, the data generated may not necessarily be reflective of CNS exposure, as BBB transport has been measured over a short experimental period using the *in situ* carotid artery technique (15).

The aim of this study, therefore, was to develop a global computational model, i.e. an *in silico* model with the ability to predict the CNS exposure (and not BBB transport alone) of any new small drug-like structure regardless of its chemical properties and simply based on its calculated molecular descriptors. The availability of such a model would be extremely useful early on in the drug discovery setting, as the CNS exposure could be predicted at a time when the major factor contributing to the CNS exposure profile (e.g. passive or active transport across the BBB or extent of plasma protein binding) would not be known. In order to undertake this assessment, it was necessary to develop a deliberate *in vivo* dataset using a range of compounds whose brain uptake is governed by processes known to be important for CNS exposure, including passive diffusion, active transport (influx and efflux) and high binding to plasma proteins (i.e. low fraction unbound present to permeate the BBB) (Table I). While it is possible to generate a dataset for BBB penetration using an *in situ* carotid artery perfusion technique (22), this technique does not consider the potential impact of plasma protein binding on CNS exposure, and is more indicative of rate of BBB penetration. For this reason, we chose to measure CNS exposure using the mouse brain uptake assay (MBUA), a technique commonly employed within the pharmaceutical industry for early preclinical assessment of brain exposure (23,24). Results obtained from the MBUA have been shown to be comparable to those obtained using the brain uptake index and *in situ* perfusion techniques (24). The brain-to-plasma (B:P) ratios for our compounds, together with rapidly calculated molecular descriptors, were subjected to PLS analysis to develop a computational model correctly sorting compounds into the groups of "high CNS exposure" (B:P > 0.3) and "low CNS exposure" (B:P < 0.3). The cut-off value of 0.3 was chosen as it reflects the approach used by the pharmaceutical industry when applying the MBUA (24). The model was validated using an external literature dataset of 251 compounds for which at least semi-quantitative values of B:P were obtained in rodents, primates and humans (Supplementary Material Table SI).

MATERIALS AND METHODS

Materials

[^{3}H]Arginine, [^{3}H]colchicine, [^{3}H]diazepam, [^{3}H]digoxin, [^{3}H]estradiol, [^{3}H]glycine, [^{3}H]imipramine, [^{3}H]propranolol, [^{3}H]tamoxifen, [^{3}H]verapamil, [^{14}C]caffeine, [^{14}C]glucose, [^{14}C]lactic acid, [^{14}C]linoleic acid, [^{14}C]mannitol, [^{14}C]oleic acid and [^{14}C]phenytoin were purchased from Perkin Elmer (Boston, MA), [^{3}H]decanoic acid, and [^{14}C]antipyrine were purchased from Sigma Aldrich (St. Louis, MO), [^{3}H]cyclosporine A, [^{3}H]dopamine, [^{3}H]hypoxanthine, [^{14}C]L-alanine and [^{14}C]L-leucine were purchased from Amersham Biosciences (Buckinghamshire, England), [^{3}H]arachidonic acid, [^{3}H]carnitine, [^{3}H]loperamide, [^{3}H]quinidine, [^{14}C]cholesterol, [^{14}C]inulin, [^{14}C-ibuprofen], [^{14}C]naproxen and [^{14}C]sucrose were obtained from American Radiolabeled Chemicals, Inc. (St. Louis, MO), and [^{14}C]linolenic acid, [^{14}C]palmitic acid, [^{3}H]saquinavir, [^{14}C]urea and [^{3}H]valproic acid were purchased from Moravek Biochemicals (Boston, MA). The specific activities and the sites of the radiolabel on each of these probe compounds

Table I Brain-to-Plasma (B:P) Ratios of Each Compound 5 min After Intravenous Dosing to Swiss Outbred Mice (Mean ± SD, *n*=3–4), Together with Proposed Mechanism Contributing to BBB Transport and CNS Exposure

Compound	Proposed factor mediating BBB transport	B:P ratio	MW (Da)	$logD_{pH\ 7.4}$	Polar surface area ($Å^2$)	No. of freely rotating bonds	No. of H-bond donors	No. of H-bond acceptors
Alanine	Active uptake	0.34 ± 0.08	89.09	−2.84	63.30	1	2	3
Amantadine	Active uptake	5.35 ± 0.95	151.25	−0.19	26.00	0	1	1
Antipyrine	Passive diffusion	0.92 ± 0.19	188.23	0.69	26.90	1	1	2
Arachidonic acid	High plasma protein binding	0.51 ± 0.20	304.47	4.02	37.30	14	1	2
Arginine	Active uptake	0.58 ± 0.03	174.20	−3.50	128.00	5	4	6
Artemether	Passive diffusion	2.65*	298.37	3.02	46.20	1	0	5
Artemisinin	Passive diffusion	2.92 ± 0.80	282.33	2.61	54.00	0	0	5
Caffeine	Passive diffusion	0.97 ± 0.30	194.19	−0.08	61.80	0	0	3
Carnitine	Combined active uptake and efflux	0.05 ± 0.002	162.21	−3.32	57.50	4	2	3
Cholesterol	Efflux	0.21 ± 0.16	386.65	8.30	20.20	5	1	1
Colchicine	Efflux	0.21 ± 0.02	399.44	1.18	83.10	6	1	7
Colistin	Passive diffusion	0.02 ± 0.01	1160.71	−4.07	491.00	32	18	29
Cyclosporine A	Efflux	0.18 ± 0.02	1202.61	2.93	279.00	15	5	23
Decanoic acid	Passive diffusion	1.53 ± 0.25	172.26	1.52	37.30	8	1	2
Diazepam	Passive diffusion	3.14 ± 1.32	284.74	2.88	32.70	0	0	3
Digoxin	Efflux	0.02 ± 0.01	780.94	1.40	203.00	7	6	14
Dihydroartemisinin	Passive diffusion	5.67 ± 1.33	248.35	2.35	57.20	0	1	5
Dopamine	Passive diffusion	0.19 ± 0.03	153.18	−1.55	66.50	2	3	3
Estradiol	High plasma protein binding	0.43 ± 0.02	272.38	3.58	40.50	0	2	2
Glucose	Active uptake	0.54 ± 0.15	180.16	−2.33	110.00	1	5	6
Glycine	Active uptake	0.55 ± 0.07	75.07	−3.15	63.30	1	2	3
Hypoxanthine	Active uptake	0.78 ± 0.03	136.11	−0.82	74.40	0	2	3
Ibuprofen	High plasma protein binding	0.01 ± 0.003	206.28	0.98	37.30	4	1	2
Imipramine	Passive diffusion	8.40 ± 0.69	280.41	3.25	6.48	4	0	2
Lactic acid	Active uptake	0.80 ± 0.21	90.08	−2.46	57.50	1	1	2
Leucine	Active uptake	0.63 ± 0.42	131.17	−1.76	63.30	3	2	3
Linoleic acid	High plasma protein binding	0.76 ± 0.04	280.45	4.29	37.30	14	1	2
Linolenic acid	High plasma protein binding	0.87 ± 0.22	278.43	3.68	37.30	13	1	2
Loperamide	Efflux	0.03 ± 0.02	477.04	4.64	43.80	8	1	4
Mannitol	Passive diffusion	0.03 ± 0.004	182.17	−2.5[c]	121.00	5	6	6
Naproxen	High plasma protein binding	0.03 ± 0.01	230.26	0.45	46.50	3	1	3
Oleic acid	High plasma protein binding	0.78 ± 0.15	282.46	4.88	37.30	15	1	2
Palmitic acid	High plasma protein binding	0.91 ± 0.50	256.42	4.52	37.30	14	1	2
Phenytoin	Efflux	0.80 ± 0.08	252.27	2.04	58.20	2	2	4
Propranolol	Passive diffusion	4.29 ± 0.45	259.34	1.16	41.50	6	2	3
Quinidine	Efflux	0.09 ± 0.03	324.42	2.26	45.60	4	1	4
Rimantadine	Active uptake	17.38 ± 1.20	179.3	0.07	26.00	1	1	1
Saquinavir	Efflux	0.14 ± 0.11	670.84	4.16	167.00	15	5	11
Sucrose	Passive diffusion	0.02 ± 0.003	342.30	−2.91	190.00	5	8	11
Tamoxifen	High plasma protein binding	0.39 ± 0.03	371.51	5.65	12.50	5	0	2
Urea	Passive diffusion	0.09 ± 0.02	60.06	−1.38	69.10	0	2	3
Valproic acid	Efflux	0.03 ± 0.003	144.21	0.42	37.30	5	1	2
Verapamil	Efflux	0.47 ± 0.02	454.60	3.86	64.00	14	0	6

$logD_{pH7.4}$, polar surface area, number of freely rotating bonds (terminal bonds excluded), number of H-bond donors and number of H-bond acceptors were calculated with ADMETPredictor (SimulationsPlus, CA)

Where available, the mechanism of transport across the BBB has been reported. For dihydroartemisinin and artemisinin, the mechanism of transport across intestinal cells has been reported, and given the similar structure of artemether to these two compounds, a passive diffusion process has been proposed. Given that dopamine exhibits limited BBB permeability, and it is not a substrate of an efflux transporter or highly plasma protein bound, it has been classified in the "passive diffusion" group (26–52)

*Data obtained from *n*=2 mice

are reported in Supplementary Material (Table SII). Artemisinin was purchased from Aldrich Chemical Company (Milwaukee, WI), amantadine, artemether, dihydroartemisinin and rimantadine were purchased from Sigma (St. Louis, MO), and colistin sulfate was purchased from Zhejiang Shenghua Biok Biology Co., Ltd (EP5 grade, Zhejiang, China). Solvable™ and Ultima Gold™ were purchased from Perkin Elmer (Boston, MA). Ketamine hydrochloride (Parnell Ketamine Injection) was obtained from Parnell Laboratories (New South Wales, Australia) and xylazine hydrochloride (Ilium Xylazil-100) was obtained from Troy Laboratories Pty. Ltd. (New South Wales, Australia).

Brain Uptake of Drugs and Drug-like Molecules

All animal studies were performed in accordance with the Australian and New Zealand Council for the Care of Animals in Research and Training Guidelines and the study protocol was approved by the Monash Institute of Pharmaceutical Sciences Animal Ethics Committee. Male Swiss Outbred mice (6–8 weeks of age; Monash Animal Services) were administered a 50 μL solution of compound by tail vein injection using a Terumo 0.5 mL insulin syringe (29 G×½″, Terumo Medical Corporation, Elkton, MD) to obtain a nominal dose of 2 μCi (for radiolabelled compounds) or 5–10 mg/kg (for unlabelled compounds) depending on solubility limitations. All compounds were administered in 0.9%w/v NaCl, however, due to poor aqueous solubility, artemisinin and dihydroartemisinin were delivered in a vehicle containing 80%v/v propylene glycol and 20%v/v DMSO, and artemether was delivered in an aqueous vehicle containing 40%v/v propylene glycol, 10% v/v ethanol and 5%v/v Solutol. At these doses, these organic vehicles have been shown not to alter the brain distribution of marker compounds (24). At 5 min post-dose, blood was collected by cardiac puncture (n=3–4 mice) and the whole brain was removed by making an incision through the back of the skull. Mice were anaesthetised approximately 3–4 min prior to blood and brain harvest with an intraperitoneal injection of ketamine and xylazine (133 mg/kg and 10 mg/kg, respectively). Whole blood (500–1000 μL) was collected into 1.5 mL Eppendorf tubes containing heparin sodium and centrifuged for 5 min at 6,700g.

Determination of Compound Concentration in Plasma and Brain Homogenate

If the compound that had been administered to mice was radiolabelled, the following processing was undertaken. A 50 μL aliquot of plasma supernatant was removed and placed into a 6 mL polyethylene scintillation vial followed by the addition of 2 mL of Ultima Gold™ scintillation cocktail and subsequent analysis by liquid scintillation counting (Tri-Carb 2800TR liquid scintillation analyser, Perkin Elmer, Boston, MA). The whole brain (with cerebellum removed) was placed into a preweighed 20 mL polyethylene scintillation vial and 2 mL of Solvable™ was added to the vial, which was maintained at 50°C overnight to ensure total tissue solubilization. To remove colour formed during tissue solubilization, 200 μL of 30%v/v hydrogen peroxide was added to the vial, which was then maintained at 50°C for a further 30 min to ensure complete decolourization. 10 mL of Ultima Gold™ scintillation cocktail was added to each vial, followed by vortexing and analysis for radioactivity by liquid scintillation counting.

When colistin, amantadine or rimantadine were administered to mice, a 50 μL aliquot of plasma was subjected to HPLC, as previously described (25,26). The brain was homogenized in a volume of milli-Q water (in mL) equal to twice or thrice the weight (in g) of the tissue, followed by precipitation with acetonitrile and subjected to HPLC or LCMS, as described previously (25,26).

When artemisinin, artemether and dihydroartemisinin were administered to mice, the plasma and brain (homogenized in 3 parts water by weight) were subsequently analysed for compound using LCMS. Mass spectrometry was performed on a Micromass ZQ single quadrupole instrument coupled with a Waters 2795 HPLC (Waters, Milford, MA) with analytical separations performed on a 50×2 mm, 2.5 μm Phenomenex Synergi Polar reverse phase column (Torrance, CA) using diazepam as an internal standard. Samples of 10 μL were applied to the column, which was maintained at 40°C within the autosampler compartment. Compounds were eluted using a ternary gradient solvent system consisting of Milli-Q water (solvent A), acetonitrile (solvent B) and ammonium formate 0.1 M in water adjusted to pH 3 (solvent C). The gradient profile for each compound was 0.0–0.45 min: 2%B; 0.45–0.5 min: 2–40%B; 0.5–5.0 min: 40–60% B; 5.0–5.5 min: 60–95%B; 5.5–6.5 min: 95%B; 6.5–7.0 min, 95–2%B, followed by a 2 min equilibration at initial gradient conditions. Solvent C was always maintained at 5%. Mass spectrometry was performed with positive mode electrospray ionization with a capillary voltage of 3.2 kV and compound specific source cone voltages (15 eV for artemisinin and 17 eV for dihydroartemisinin and artemether) with monitoring occurring at m/z of 283.1 for artemisinin and m/z of 267.4 for dihydroartemisinin and artemether. Source block and desolvation temperatures of 90°C and 350°C were maintained, with a desolvation gas flow rate of 350 L/h. The lowest limit of quantitation (LLQ) for the plasma and brain homogenate assay of each compound, determined by the lowest concentration exhibiting precision less than 20% and accuracy in the range of 80–120% from replicate analyses of 3–6 quality control samples, ranged from 25 to 500 ng/mL or ng/g. The values of precision for these assays ranged between 4.7% and 8.4%

and the values for the accuracy of these assays ranged between 92.2% and 108.3%. Data acquisition, peak integration and calculations were performed using Micromass Masslynx version 4.1 software. The concentration of compound in plasma and brain samples obtained from brain uptake studies was determined using a calibration curve relating peak area to standard solution concentration.

Determination of Brain Vascular Plasma Volume

To determine the volume of plasma present within the brain microvasculature (subsequently required for data analysis), a 50 μL solution of [^{14}C]inulin (0.04 μCi/μL in 0.9%w/v NaCl) was administered to mice by tail vein injection, and brain and plasma samples were collected 5 min post-dose and processed by liquid scintillation counting. Given the molecular weight of inulin (5000 Da) and its inability to permeate the BBB, any radioactivity present within brain homogenate following administration of [^{14}C]inulin is assumed to be associated with the brain microvasculature plasma, providing an estimate of the brain microvascular plasma volume.

Calculation of Brain-to-Plasma Ratio

The concentration of compound in the brain vasculature ($C_{brain\ vasculature}$, ng/g) was determined by multiplying the concentration of compound in the plasma (C_{plasma}, ng/mL) by the plasma volume of the brain vasculature (V_p, mL/g), as shown in Eq. 1. The plasma volume of the brain vasculature was 26±6 μL/g of brain tissue (mean ± SD, n=8), assessed following intravenous administration of [^{14}C]inulin.

$$C_{brain\ vasculature} = C_{plasma} * V_p \quad (1)$$

The concentration of compound in the brain parenchyma (C_{brain}, ng/g) could then be determined by the difference between the concentration of compound detected in the brain homogenate ($C_{brain\ homogenate}$, ng/g) and the concentration of compound in the brain vasculature (Eq. 2).

$$C_{brain} = C_{brain\ homogenate} - C_{brain\ vasculature} \quad (2)$$

A brain-to-plasma (B:P) ratio was then calculated by comparing the concentration of compound in the brain parenchyma (C_{brain}, ng/g) to the concentration of compound in the plasma (C_{plasma}, ng/mL) (Eq. 3), with the assumption that 1 g of brain tissue is equivalent in density to 1 mL of plasma (23).

$$B:P = \frac{C_{brain}}{C_{plasma}} \quad (3)$$

Molecular Descriptors and Model Development

Physicochemical properties and molecular descriptors were calculated with ADMETPredictor 5.0 (SimulationsPlus, CA) and DragonX 1.4 (Talete, Italy). The descriptors were used to identify structural diversity within the dataset and to analyze which molecular features were linked to CNS exposure. Structural diversity was confirmed with Principal Component Analysis (PCA); the experimental dataset was assessed by superimposing the compounds on the oral drug-space. The dataset was found to be drug-like with only palmitic acid and colistin being significant outliers from the drug-like chemical space (Fig. 1). The relationship between molecular descriptors and CNS exposure, in the form of the $\log_{10}$ of the B:P ratio, was established using partial least squares projection to latent structures (PLS) (Simca-P 11.0, Umetrics, Sweden). In the PLS model development, the descriptors were de-identified to not bias the variable selection. In addition, standard pre-processing of the descriptors was performed with all descriptors being mean centered to improve the interpretability of the model and scaled to unit variance to prevent descriptors that are quantitatively larger from dominating the model. After removal of skewed descriptors and descriptors with zero variance, a matrix consisting of 812 descriptors was submitted for PLS. With the aim to maintain predictivity and increase the robustness of the model, a variable selection was performed in which descriptors that were not directly related to the response were excluded (thus reducing noise). Firstly, all descriptors except the 100 with highest importance for the response were excluded. Secondly, variables with low or little influence on the model, as identified by the variable of importance plot, and highly correlated variables that duplicated the information contained within other variables (residing in the same area of the PLS loading plot) were excluded to leave a few variables representing the key properties that encoded the majority of the information related to CNS exposure. All compounds for which experimental data was generated were included in the model development to allow maximum structural information to influence the model. Therefore, the variable selection process was monitored by the R^2, the cross-validated R^2 (Q^2 using 7 cross validation groups) and the root mean squared error of the estimate (RMSEE). The models were validated by permutation tests (100 iterations) in which the values for the response variable were randomized and the multivariate data analysis was repeated to detect whether chance correlations had occurred. The final model consisted of five non-correlated (R of 0.03–0.47 in the correlation matrix), significant variables. This model was challenged with a test set of 251 compounds for which semi-quantitative B:P values were found in the literature (see Supplementary Material Figure S1 and Table SI). To establish this dataset, an in-

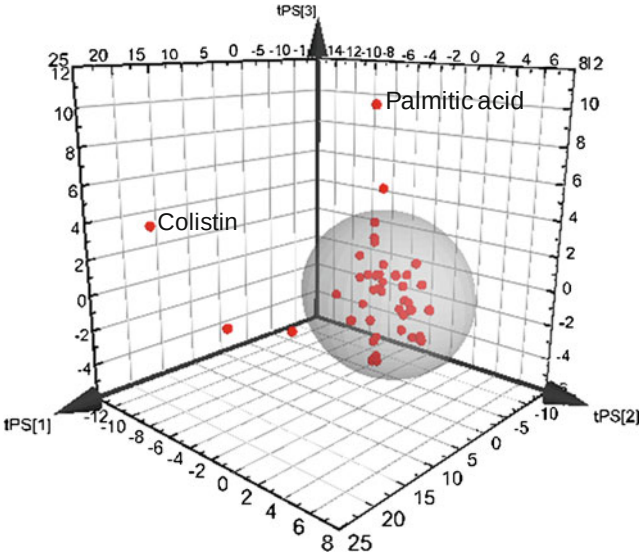

Fig. 1 Structural diversity and drug-likeness of the dataset used for model development. The 95% confidence interval of the first three principal components (PC) of the oral drug space (explaining 72% of the chemical variation of orally administered drugs) is shown by the grey sphere. Orally-administered drugs marketed in Sweden (n=477) were used to extract the oral drug space onto which the dataset used in this study was super-imposed (red circles) to analyse the chemical diversity. The dataset was judged as being structurally diverse and drug-like. However, palmitic acid and colistin were shown to be significant outliers in the distance to model analysis in all PCs extracted for the oral drug space.

house dataset of 461 marketed drugs (440 orally and 21 parenterally administered drugs) was used as the primary list for which we sought information about CNS exposure. Stringent search criteria were used for inclusion of compounds to obtain as accurate a classification of the compounds as possible. The selection criteria were based on reported B:P ratios or a clear reported indication of the extent of compound reaching or not reaching the brain—as an example, statements such as 'does not permeate the BBB' were considered acceptable for classification into the low CNS exposure group. We did not include compounds that have been classified as CNS active if it was not possible to obtain data supporting the extent to which the compound distributes into the brain. This approach was taken so as not to bias the CNS exposure model by measures of, or information about, pharmacological activity in the brain. The chemical space covered by the training set was shown to cover that of the test set (Supplementary Material, Figure S1) and hence, it was regarded as appropriate for testing the final CNS exposure model.

Statistical Analyses

Significant differences in the distribution of physicochemical properties were assessed using two-tailed Mann Whitney non parametric tests ($p<0.05$) (Prism, GraphPad, version 5.04). The accuracy of *in silico* classifications (% of the compounds) was calculated by

$$\text{Accuracy} = \frac{TP + TN}{TP + FP + TN + FN} \times 100 \quad (4)$$

where TP is true positive (high CNS exposure), FP is false positive, TN is true negative (low CNS exposure) and FN is false negative. The precision of the prediction, the sensitivity and specificity were calculated by

$$\text{Positive precision} = \frac{TP}{TP + FP} \quad (5)$$

$$\text{Negative precision} = \frac{TN}{TN + FN} \quad (6)$$

$$\text{Sensitivity} = \frac{TP}{TP + FN} \quad (7)$$

$$\text{Specificity} = \frac{TN}{TN + FP} \quad (8)$$

where positive precision is the precision of prediction of high CNS exposure and negative precision is that of the low CNS exposure predictions.

RESULTS AND DISCUSSION

The 5 min post-dose B:P ratio of each probe compound, together with the associated physicochemical properties and the proposed factors affecting CNS exposure, are summarised in Table I. The proposed mechanisms of transport across the BBB were all taken from literature, however, in some instances where BBB transport mechanisms were not available (e.g. for the artemisinin-based antimalarial drugs), data obtained from intestinal absorption studies were used to predict the mechanism of transport across the BBB (26–52). In addition to including compounds which permeate the BBB by passive diffusion, we ensured that our computational CNS exposure model was designed to deliberately include actively transported compounds in the dataset. We did so to explore the possibility of establishing a truly general model for CNS exposure, applicable to early virtual screening before prior knowledge of transport mechanisms are obtained. We decided to design the dataset so that equal weight was given to compounds which permeate the BBB passively, are substrates for BBB transporters and whose CNS access is likely to be limited by plasma protein binding. In our experimental dataset, 35% of the compounds were proposed to access the brain by passive

diffusion whereas 21% of the compounds were proposed to employ influx transporters. For 23% of the compounds, access to the brain was limited by the function of BBB efflux transporters and the CNS exposure of 21% of compounds was proposed to be limited by plasma protein binding.

In general, compounds which permeate the BBB via passive diffusion demonstrated the highest B:P ratios (e.g. propranolol with a B:P ratio of 4.29±0.45 and imipramine with a B:P ratio of 8.40±0.69), whereas compounds which are substrates for a known efflux transporter (e.g. digoxin and valproic acid) or are highly plasma-protein bound (e.g. ibuprofen and naproxen) demonstrated the lowest brain uptake following systemic administration. Compounds which are substrates for known active transport processes (e.g. alanine and glucose) had intermediate B:P values. Hence, the MBUA assay successfully ranked the brain uptake of probe compounds in the general permeability order of passive compounds > active transport substrates > efflux substrates = compounds with high plasma protein binding, in an order which is consistent with literature (23). One of the major advantages of this model compared with the *in situ* carotid artery perfusion model, is that the brain uptake of compounds is assessed in an intact physiological system, and in the presence of plasma proteins and other plasma-derived factors which may impact on overall brain disposition. Additionally, active transport proteins which are involved in active uptake or efflux are not down regulated, as can be observed when using *in vitro* cell culture models (8). Therefore, this *in vivo* model assesses brain uptake under physiologically-relevant conditions and is able to discriminate between compounds whose brain uptake is limited by active uptake, active efflux, as well as high plasma protein binding.

It is well-known that increased lipophilicity drives increased CNS exposure if compounds are passively absorbed (14–16). Figure 2 demonstrates the relationship between lipophilicity of probe compounds and brain uptake, and as expected for compounds permeating the BBB via passive diffusion, a linear relationship exists between B:P ratios and $\log D_{pH7.4}$ (R^2 of 0.93). Compounds exhibiting active uptake across the BBB display a higher B:P ratio than that predicted by their lipophilicity, whereas compounds which are substrates for efflux transport systems or are highly plasma protein bound exhibit a B:P ratio substantially lower than that predicted by their lipophilicity. While such phenomena have been observed previously (15,53), the current dataset shows a greater disparity between passively and non-passively absorbed compounds, and uses B:P ratio in place of PS (a permeability-surface area coefficient measured by the *in situ* carotid artery technique), thereby including compounds whose brain uptake is also limited by high plasma protein binding.

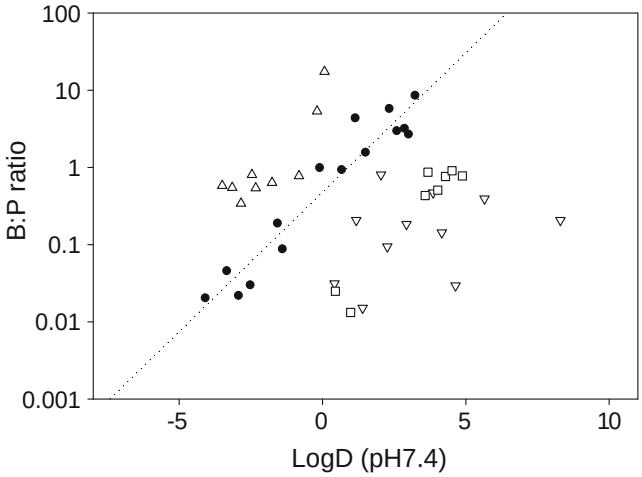

Fig. 2 Relationship between $\log D_{pH\ 7.4}$ and 5 min post-dose brain-to-plasma (B:P) ratio**.** Compounds in this dataset are classified as permeating the BBB by passive diffusion (●), being substrates for active influx transporters (Δ), being substrates for active efflux transporters (∇) or being highly plasma protein bound (□). The linear regression for compounds for which CNS exposure is only affected by passive diffusion across the BBB is shown (R^2=0.93).

While a clear relationship between lipophilicity and CNS exposure existed for those compounds accessing the BBB by simple passive diffusion, no relationship was evident between any previously suggested BBB permeability descriptors (e.g. $\log D_{pH7.4}$, PSA, number of rotatable bonds, molecular size) and CNS exposure when all compounds in our dataset were included. However, when we classified compounds into "low CNS exposure" or "high CNS exposure" groups, some evident relationships between extent of CNS exposure and physicochemical properties emerged (Fig. 3). It was observed that the PSA and number of freely rotatable bonds were significantly lower for the group of compounds with high CNS exposure, whereas lipophilicity, molecular weight and asphericity appeared not to differ between both groups. This suggested the possibility that extent of CNS exposure could be predicted based on molecular structure. To this end, we explored whether multivariate analysis could further predict extent of CNS exposure from molecular structural parameters.

We used the $\log_{10}$ of the B:P ratio and developed a PLS model which after variable selection contained five molecular descriptors calculated with the program DragonX. These were (in order of importance): the maximum electrotopological negative variation (MAXDN), the folding degree index (FDI), the 3D-MoRSE signal 15 weighted by Sanderson´s electronegativity (MOR15e), the 2nd component shape directional WHIM index weighted by atomic polarisability (P2p) and the mean topological charge index of order 8 (JGI8). The descriptors resulted in a model that was valid as assessed by Q^2 and permutation test, however, the statistics were modest (R^2 of 0.57, Q^2 of 0.52, RMSEE

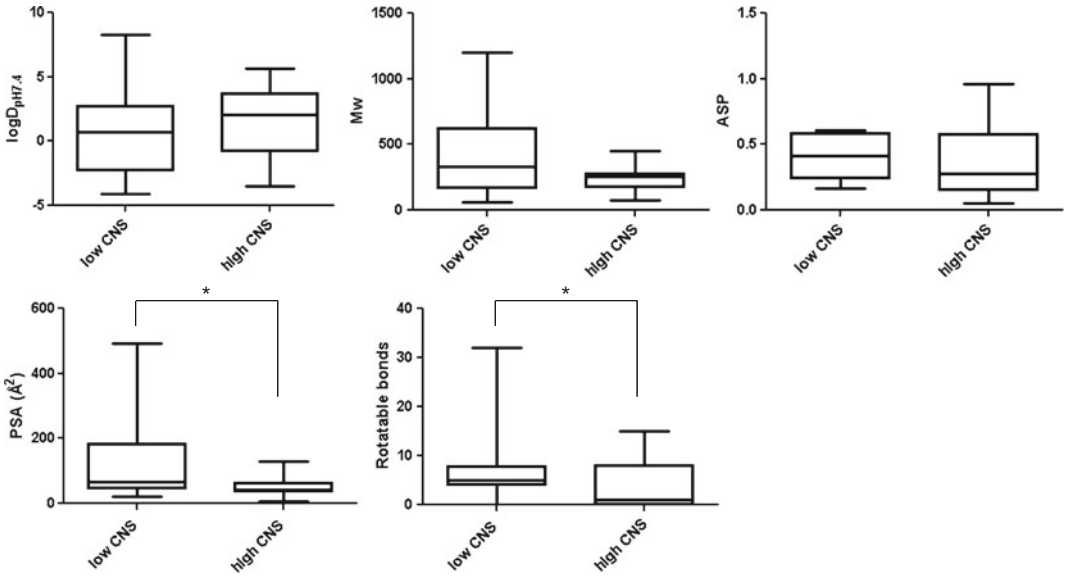

Fig. 3 Differences in physicochemical properties between the "low CNS exposure" and "high CNS exposure" groups. Significantly different values were obtained for polar surface area (PSA) and number of rotatable bonds ($p < 0.05$). Lipophilicity, molecular weight and asphericity (ASP; a shape descriptor) were not significantly different between the groups.

of 0.53; Table II). We therefore chose to use the resulting model in a qualitative mode which sorted compounds into the "high CNS exposure" and "low CNS exposure" classes (Fig. 4, Table III). This strategy has previously shown to be successful when predicting another complex property, the melting point of drugs (54). In addition, it enabled us to use a large semi-quantitative test set for the external validation. It was shown that 74% of the training set was accurately predicted, and indeed, better sorting was obtained for the external test set for which 76% of the predictions were accurate. The precision of the predictions, the sensitivity and selectivity are presented in Table II.

Table II Statistics for the PLS Model in the Quantitative and Qualitative Mode

	Quantitative Model	Class Model Tr set	Class Model Te set
R^2	0.57		
Q^2	0.52		
$RMSEE_{tr}$	0.53		
MAXDN	−0.35		
FDI	0.30		
3D-MOR15e	−0.24		
P2p	0.24		
JGI8	−0.23		
Constant	−0.53		
Accuracy (%)		74	76
Positive precision		0.81	0.79
Negative precision		0.67	0.73
Sensitivity		0.78	0.75
Specificity		0.69	0.81

Statistics from the PLS analysis represented by the coefficient of determination (R^2), leave-one-out cross-validated R^2 (Q^2), the root mean square error of the estimation of the training set ($RMSEE_{tr}$), and the PLS coefficients from the final model (using scaled and centered descriptors) are shown.

Accuracy, precision, sensitivity and selectivity were calculated as described in Eqs. 4–8. tr denotes training set (n=43), te denotes test set (n=251).

Although the BBB permeability of drugs has been extensively modelled, the CNS exposure has, due to its complexity, rarely been used as the response variable. Recently, researchers at AstraZeneca published *in silico* approaches to predict the unbound brain-to-plasma concentration ($K_{p,uu,brain}$) using QSAR (55) and machine learning algorithms (56). Their first attempts were based on 43 drugs and drug metabolites (included in our external test set) and they utilised 16 commonly used descriptors (hydrogen bond properties, lipophilicity, size, flexibility, ionization properties) to develop models for prediction of the B:P ratio and $K_{p,uu,brain}$. A model based on hydrogen bond acceptors, $logD_{pH7.4}$, and descriptors for acids and bases was developed for the B:P ratio, resulting in a Q^2 of 0.69. When we used similar descriptors calculated with the descriptor programs used herein to predict our dataset, the R^2 and Q^2 values produced were only 0.25 and 0.13, respectively. In addition, the $logD_{pH7.4}$ and descriptor for acids were non-significant for our dataset. Interestingly, the model that we developed did not contain any direct lipophilicity or hydrogen bond measures, although these properties to some extent may be reflected by the descriptors included in the model. We speculate that this is a result of the rather small number of compounds in our dataset for which the CNS exposure was limited by passive diffusion only. Instead the

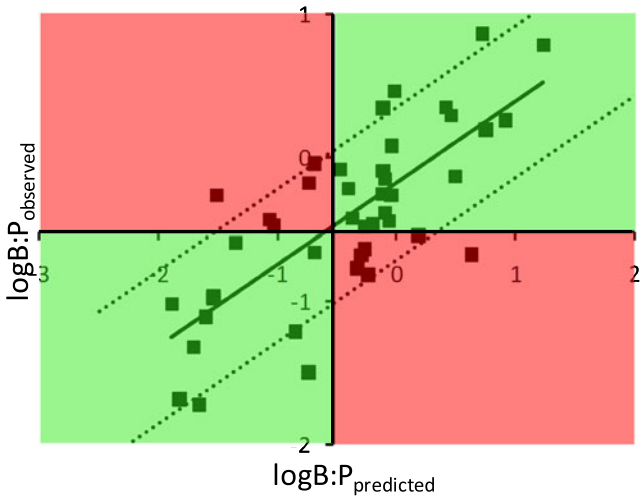

Fig. 4 Results from the computational model development. The trend line (*continuous line*) and the RMSE of the estimates of the training set (*dotted lines*) are shown. The red and green boxes demonstrate how well the compounds were predicted after transferring the model to a qualitative prediction, sorting compounds into high and low CNS exposure groups using a B:P ratio of 0.3 (corresponding to log B:P of -0.52) as a cut-off. Of the falsely predicted compounds, 36% were limited in their CNS exposure by passive diffusion, 36% by efflux, 18% by active influx and 9% (one compound) by plasma protein binding.

properties that were of importance for the CNS exposure of the current dataset were related to shape (FDI and P2p), polarisability (MAXDN and P2p), electronegativity (MAXDN and 3D-MOR15e) and charge transfer (JGI8). To interpret the exact meaning of each of these molecular properties for the resulting CNS exposure is difficult since the factors may be important for several of the processes influencing the final CNS exposure. However, the overall information captured by these molecular descriptors has been identified to be of importance for BBB membrane permeability (charge and shape) (57), BBB efflux (polarisability, shape, charge) (58,59), plasma protein binding (electronegativity) (60) and $K_{p,uu,brain}$ (shape) (56).

Based on our structurally diverse dataset with compounds whose CNS access was affected by multiple processes, we were able to develop a computational model that had the ability to separate between compounds with low and high CNS exposure using the cut-off value of B:P of 0.3. We also evaluated the utility of introducing a third, intermediate class to improve the statistics of the model, an approach we have used previously for predicting permeability (61) and melting point (54). The qualitative prediction was in this case sorted into classes based on B:P ratio of <0.3 for low CNS exposure and B:P ratio >1.0 for high CNS exposure, with intermediate exposure between these values. Overall, this did not result in improved statistics for this model, however the precision in the separation between high and low CNS exposure was significantly improved. Hence, this suggests that it would be possible to generate highly accurate classification models of high and low CNS exposure by designing a dataset in which intermediate CNS exposure drugs are excluded. Unfortunately, for the dataset studied herein, this would result in the exclusion of 18 compounds, leaving too small a dataset to allow effective model development.

Table III Predictions of 'Low CNS Exposure' and 'High CNS Exposure' of the Training Set

	$Compounds_{tr}$	$B:P_{obs}$	$B:P_{pred}$
1	Alanine	High	High
2	Amantadine	High	High
3	Antipyrine	High	High
4	Arachidonic acid	High	Low
5	Arginine	High	Low
6	Artemisinin	High	High
7	Arthemether	High	High
8	Caffeine	High	High
9	Carnitine	Low	Low
10	Cholesterol	Low	High
11	Colchicine	Low	Low
12	Colistin	Low	Low
13	Cyclosporine A	Low	Low
14	Decanoic acid	High	Low
15	Diazepam	High	High
16	Digoxin	Low	Low
17	Dihydroartemisinin	High	High
18	Dopamine	Low	High
19	Estradiol	High	High
20	Glucose	High	Low
21	Glycine	High	High
22	Hypoxanthine	High	High
23	Ibuprofen	Low	Low
24	Imipramine	High	High
25	Lactic acid	High	High
26	Leucine	High	High
27	Linoleic acid	High	High
28	Linolenic acid	High	High
29	Loperamide	Low	Low
30	Mannitol	Low	Low
31	Naproxen	Low	Low
32	Oleic acid	High	High
33	Palmitic acid	High	High
34	Phenytoin	High	High
35	Propranolol	High	Low
36	Quinidine	Low	High
37	Rimantadine	High	High
38	Saquinavir	Low	Low
39	Sucrose	Low	Low
40	Tamoxifen	Low	Low
41	Urea	Low	High
42	Valproic acid	Low	High
43	Verapamil	Low	High

To certify that the model had not been overtrained, i.e. that it was not highly specific for the dataset used for training and less accurate for other compounds, we challenged the model with an external test set. In total 251 compounds were tested and indeed, higher accuracy was obtained for the test set as compared to the training set (Table II and Supplementary Material Table SIII). This further strengthens the conclusion that the descriptors extracted in the model development are of general importance for CNS exposure. The success to predict the test set which to a large part was based on compounds for which CNS exposure was determined at steady state, also suggests that the less invasive and less time consuming *in vivo* MBUA may be used to estimate CNS exposure at steady state. This strengthens the potential applicability of the MBUA in drug screening, given the limitations associated with surgical approaches required to achieve steady state plasma (and brain) concentrations in rodents. Despite the benefits associated with the MBUA, it is limited by the fact that it provides a measure of total brain concentrations, and not free brain concentrations, which is what governs pharmacological activity. To computationally predict the pharmacological effect in the CNS, more elaborate *in silico* models would be needed, and typically such predictions need to involve a combination of several different approaches such as *in silico* $K_{p,uu,brain}$ models combined with virtual docking to CNS targets. To date, models for e.g. fraction unbound in plasma are present (e.g. included in several software including ADMETPredictor used in this study) and the first attempts to predict unbound volume of distribution in the brain and $K_{p,uu,brain}$ have been published (55,56). Unfortunately the more extensive models are trained on datasets that are not revealed and/or the final descriptors and the equations used for calculations are not disclosed (56), therefore, limiting the transferability of such models to other laboratories. In addition to models for $K_{p,uu,brain}$ and volume of distribution, computational models for prediction of active transport across the BBB are warranted to more accurately predict the amount of drug that reaches the brain.

The interplay between transporters, the possibility of transporter modulation (stimulation, inhibition) and species differences in protein expression and substrate specificity are factors that contribute to the complexity of predictions of active transport. Although the intent of this computational model was not to predict CNS exposure based on ability to be actively transported across the BBB, we are encouraged by the fact that our model predicted 70% of the actively transported compounds in our training set correctly. The corresponding numbers for the passively diffusing compounds and highly protein bound compounds are 71% and 89%, respectively. The exact meaning of each of these numbers is difficult to extract since each subgroup is relatively small, consisting of 9–14 compounds. A larger number of compounds would be required to further determine the potential of such computational models to accurately predict CNS exposure based on mechanism of transport across the BBB or the major factor contributing to CNS exposure. Nonetheless, we have developed a computational model that can accurately predict CNS exposure regardless of the major contributing factor affecting CNS access, which is of extreme benefit early on in the drug discovery setting. The methods and descriptors used herein are examples of statistical techniques and molecular descriptors that can be used to develop such models. It is likely that other computational methods, such as support vector machine and random forest algorithms (56,62,63), will also enable successful predictions of CNS exposure.

CONCLUSIONS

We have developed a computational model which correctly classifies compounds with high and low CNS exposure based on previously unexplored molecular descriptors. A novel dataset which was designed to reflect the major processes of importance to CNS exposure (passive diffusion across the BBB, active BBB influx and efflux and fraction unbound in plasma) was used to train the model and descriptors reflecting molecular shape, polarisability, electronegativity and charge transfer accurately predicted 76% of the 251 compounds in a test set used to challenge the model. This study contributes to the limited open literature on *in silico* prediction of CNS exposure and our results indicate that highly complex processes can be predicted with reasonable accuracy from rapidly calculated molecular descriptors.

ACKNOWLEDGMENTS AND DISCLOSURES

The authors would like to thank Dr. Thomas J. Raub for his assistance and guidance in development and validation of the mouse brain uptake assay. We thank SimulationsPlus (Lancaster, CA) for providing the Department of Pharmacy, Uppsala University, with a reference site license for the software ADMET Predictor. Financial support from the Swedish Agency for Innovation Systems (Grant 2010-00966) for Christel Bergström's Marie Curie Fellowship at Monash University is gratefully acknowledged.

REFERENCES

1. Reese TS, Karnovsky MJ. Fine structural localization of a blood-brain barrier to exogenous peroxidase. J Cell Biol. 1967;34:207–17.
2. Brightman MW, Reese TS. Junctions between intimately apposed cell membranes in the vertebrate brain. J Cell Biol. 1969;40:648–77.
3. Eyal S, Hsiao P, Unadkat JD. Drug interactions at the blood-brain barrier: fact or fantasy? Pharmacol Ther. 2009;123:80–104.
4. Ghersi-Egea JF, Leininger-Muller B, Cecchelli R, Fenstermacher JD. Blood-brain interfaces: relevance to cerebral drug metabolism. Toxicol Lett. 1995;82–83:645–53.

5. Pardridge WM. Crossing the blood-brain barrier: are we getting it right? Drug Discov Today. 2001;6:1–2.
6. Pardridge WM. William Pardridge discusses the lack of BBB research. Interview by Rebecca N. Lawrence. Drug Discov Today. 2002;7:223–6.
7. Bickel U. How to measure drug transport across the blood-brain barrier. NeuroRx. 2005;2:15–26.
8. Gumbleton M, Audus KL. Progress and limitations in the use of *in vitro* cell cultures to serve as a permeability screen for the blood-brain barrier. J Pharm Sci. 2001;90:1681–98.
9. Nicolazzo JA, Charman SA, Charman WN. Methods to assess drug permeability across the blood-brain barrier. J Pharm Pharmacol. 2006;58:281–93.
10. Van Dorpe S, Bronselaer A, Nielandt J, Stalmans S, Wynendaele E, Audenaert K, *et al.* Brainpeps: the blood-brain barrier peptide database. Brain Struct Funct. In press; (2011).
11. Kerns EH, Di L. Blood-brain barrier methods. Drug-like properties: Concepts, structure design and methods from ADME to toxicity optimization. Burlington: Academic; 2008. p. 311–28.
12. Clark DE. *In silico* prediction of blood-brain barrier permeation. Drug Discov Today. 2003;8:927–33.
13. Goodwin JT, Clark DE. *In silico* predictions of blood-brain barrier penetration: considerations to "keep in mind". J Pharmacol Exp Ther. 2005;315:477–83.
14. Levin VA. Relationship of octanol/water partition coefficient and molecular weight to rat brain capillary permeability. J Med Chem. 1980;23:682–4.
15. Liu X, Tu M, Kelly RS, Chen C, Smith BJ. Development of a computational approach to predict blood-brain barrier permeability. Drug Metab Dispos. 2004;32:132–9.
16. Young RC, Mitchell RC, Brown TH, Ganellin CR, Griffiths R, Jones M, *et al.* Development of a new physicochemical model for brain penetration and its application to the design of centrally acting H2 receptor histamine antagonists. J Med Chem. 1988;31:656–71.
17. Kelder J, Grootenhuis PD, Bayada DM, Delbressine LP, Ploemen JP. Polar molecular surface as a dominating determinant for oral absorption and brain penetration of drugs. Pharm Res. 1999;16:1514–9.
18. Osterberg T, Norinder U. Prediction of polar surface area and drug transport processes using simple parameters and PLS statistics. J Chem Inf Comput Sci. 2000;40:1408–11.
19. van de Waterbeemd H, Camenisch G, Folkers G, Chretien JR, Raevsky OA. Estimation of blood-brain barrier crossing of drugs using molecular size and shape, and H-bonding descriptors. J Drug Target. 1998;6:151–65.
20. Ajay A, Bemis GW, Murcko MA. Designing libraries with CNS activity. J Med Chem. 1999;42:4942–51.
21. Garg P, Verma J. *In silico* prediction of blood brain barrier permeability: an artificial neural network model. J Chem Inf Model. 2006;46:289–97.
22. Takasato Y, Rapoport SI, Smith QR. An *in situ* brain perfusion technique to study cerebrovascular transport in the rat. Am J Physiol. 1984;247:H484–93.
23. Garberg P, Ball M, Borg N, Cecchelli R, Fenart L, Hurst RD, *et al.* *In vitro* models for the blood-brain barrier. Toxicol *In Vitro*. 2005;19:299–334.
24. Raub TJ, Lutzke BS, Andrus PK, Sawada GA, Staton BA. Early preclinical evaluation of brain exposure in support of hit identification and lead optimization. In: Borchardt RT, Kerns EH, Hageman M, Thakker DR, Stevens JL, editors. Optimizing the "Drug-Like" properties of leads in drug discovery. Hoboken: Spinger; 2006. p. 355–410.
25. Jin L, Li J, Nation RN, Nicolazzo JA. Brain penetration of colistin in mice assessed by a novel high-performance liquid chromatographic technique. Antimicrob Agents Chemother. 2009;53:4247–51.
26. Kooijmans SA, Senyschyn D, Mezhiselvam MM, Morizzi J, Charman SA, Weksler B, *et al.* The involvement of a Na+ and Cl–dependent transporter in the brain uptake of amantadine and rimantadine. Mol Pharmaceut. 2012;9:883–93.
27. Oldendorf WH. Lipid solubility and drug penetration of the blood brain barrier. Proc Soc Exp Biol Med. 1974;147:813–5.
28. Smith QR, Momma S, Aoyagi M, Rapoport SI. Kinetics of neutral amino acid transport across the blood-brain barrier. J Neurochem. 1987;49:1651–8.
29. Oldendorf WH, Szabo J. Amino acid assignment to one of three blood-brain barrier amino acid carriers. Am J Physiol. 1976;230:94–8.
30. Augustijns P, D'Hulst A, Van Daele J, Kinget R. Transport of artemisinin and sodium artesunate in Caco-2 intestinal epithelial cells. J Pharm Sci. 1996;85:577–679.
31. Hamilton JA, Hillard CJ, Spector AA, Watkins PA. Brain uptake and utilization of fatty acids, lipids and lipoproteins: application to neurological disorders. J Mol Neurosci. 2007;33:2–11.
32. Richieri GV, Kleinfeld AM. Unbound free fatty acid levels in human serum. J Lipid Res. 1995;36:229–40.
33. Nakanishi T, Hatanaka T, Huang W, Prasad PD, Leibach FH, Ganapathy ME, *et al.* Na+- and Cl–coupled active transport of carnitine by the amino acid transporter ATB0,+ from mouse colon expressed in HRPE cells and Xenopus oocytes. J Physiol. 2001;532:297–304.
34. Tamai I, Ohashi R, Nezu J, Yabuuchi H, Oku A, Shimane M, *et al.* Molecular and functional identification of sodium ion-dependent, high affinity human carnitine transporter OCTN2. J Biol Chem. 1998;273:20378–82.
35. Do TM, Ouellet M, Calon F, Chimini G, Chacun H, Farinotti R, *et al.* Direct evidence of abca1-mediated efflux of cholesterol at the mouse blood-brain barrier. Mol Cell Biochem. 2011;357:397–404.
36. Drion N, Lemaire M, Lefauconnier JM, Scherrmann JM. Role of P-glycoprotein in the blood-brain transport of colchicine and vinblastine. J Neurochem. 1996;67:1688–93.
37. Jin L, Li J, Nation RN, Nicolazzo JA. The impact of P-glycoprotein inhibition and lipopolysaccharide administration on the blood-brain barrier transport of colistin in mice. Antimicrob Agents Chemother. 2011;55:502–7.
38. Schinkel AH, Wagenaar E, van Deemter L, Mol CA, Borst P. Absence of the mdr1a P-Glycoprotein in mice affects tissue distribution and pharmacokinetics of dexamethasone, digoxin, and cyclosporin A. J Clin Invest. 1995;96:1698–705.
39. Oldendorf WH. Carrier-mediated blood-brain barrier transport of short-chain monocarboxylic organic acids. Am J Physiol. 1973;224:1450–3.
40. Dagenais C, Rousselle C, Pollack GM, Scherrmann JM. Development of an *in situ* mouse brain perfusion model and its application to mdr1a P-glycoprotein-deficient mice. J Cereb Blood Flow Metab. 2000;20:381–6.
41. Crowe A, Ilett KF, Karunajeewa HA, Batty KT, Davis TM. Role of P glycoprotein in absorption of novel antimalarial drugs. Antimicrob Agents Chemother. 2006;50:3504–6.
42. Bertler A, Falck B, Rosengren E. The direct demonstration of a barrier mechanism in the brain capillaries. Acta Pharmacol Toxicol. 1963;20:317–21.
43. Pardridge WM, Mietus LJ. Transport of steroid hormones through the rat blood-brain barrier. J Clin Invest. 1979;64:145–54.
44. Spector R. Hypoxanthine transport through the blood-brain barrier. Neurochem Res. 1987;12:791–6.
45. Parepally JM, Mandula H, Smith QR. Brain uptake of nonsteroidal anti-inflammatory drugs: ibuprofen, flurbiprofen, and indomethacin. Pharm Res. 2006;23:873–81.
46. Oldendorf WH. Brain uptake of radiolabeled amino acids, amines, and hexoses after arterial injection. Am J Physiol. 1971;221:1629–39.

47. Doran A, Obach RS, Smith BJ, Hosea NA, Becker S, Callegari E, *et al.* The impact of P-glycoprotein on the disposition of drugs targeted for indications of the central nervous system: evaluation using the MDR1A/1B knockout mouse model. Drug Metab Dispos. 2005;33:165–74.
48. Borgå O, Borgå B. Serum protein binding of nonsteroidal antiinflammatory drugs: a comparative study. J Pharmacokinet Biopharm. 1997;25:63–77.
49. Kurihara A, Suzuki H, Sawada Y, Sugiyama Y, Iga T, Hanano M. Uptake of propranolol by microvessels isolated from bovine brain. J Pharm Sci. 1987;76:759–64.
50. Kim RB, Fromm MF, Wandel C, Leake B, Wood AJ, Roden DM, *et al.* The drug transporter P-glycoprotein limits oral absorption and brain entry of HIV-1 protease inhibitors. J Clin Invest. 1998;101:289–94.
51. Shah IG, Parsons DL. Human albumin binding of tamoxifen in the presence of a perfluorochemical erythrocyte substitute. J Pharm Pharmacol. 1991;43:790–3.
52. Gibbs JP, Adeyeye MC, Yang Z, Shen DD. Valproic acid uptake by bovine brain microvessel endothelial cells: role of active efflux transport. Epilepsy Res. 2004;58:53–66.
53. Pardridge WM. CNS drug design based on principles of blood-brain barrier transport. J Neurochem. 1998;70:1781–92.
54. Bergström CA, Norinder U, Luthman K, Artursson P. Molecular descriptors influencing melting point and their role in classification of solid drugs. J Chem Inf Comput Sci. 2003;43:1177–85.
55. Fridén M, Winiwarter S, Jerndal G, Bengtsson O, Wan H, Bredberg U, *et al.* Structure-brain exposure relationships in rat and human using a novel data set of unbound drug concentrations in brain interstitial and cerebrospinal fluids. J Med Chem. 2009;52:6233–43.
56. Chen H, Winiwarter S, Fridén M, Antonsson M, Engkvist O. *In silico* prediction of unbound brain-to-plasma concentration ratio using machine learning algorithms. J Mol Graph Model. 2011;29:985–95.
57. Fischer H, Gottschlich R, Seelig A. Blood-brain barrier permeation: molecular parameters governing passive diffusion. J Membr Biol. 1998;165:201–11.
58. Dearden JC, Al-Noobi A, Scott AC, Thomson SA. QSAR studies on P-glycoprotein-regulated multidrug resistance and on its reversal by phenothiazines. SAR QSAR Environ Res. 2003;14:447–54.
59. Seelig A. The role of size and charge for blood-brain barrier permeation of drugs and fatty acids. J Mol Neurosci. 2007;33:32–41.
60. Lobell M, Sivarajah V. *In silico* prediction of aqueous solubility, human plasma protein binding and volume of distribution of compounds from calculated pKa and AlogP98 values. Mol Divers. 2003;7:69–87.
61. Bergström CA, Strafford M, Lazorova L, Avdeef A, Luthman K, Artursson P. Absorption classification of oral drugs based on molecular surface properties. J Med Chem. 2003;46:558–70.
62. Kortagere S, Chekmarev D, Welsh WJ, Ekins S. New predictive models for blood-brain barrier permeability of drug-like molecules. Pharm Res. 2008;25:1836–45.
63. Muehlbacher M, Spitzer GM, Liedl KR, Kornhuber J. Qualitative prediction of blood-brain barrier permeability on a large and refined dataset. J Comput Aided Mol Des. 2011;25:1095–6.